Marine Geology 395 (2018) 320–330

Contents lists available at ScienceDirect

Marine Geology

journal homepage: www.elsevier.com/locate/margo

The chronology of a sediment core from incised valley of the Yangtze River delta: Comparative OSL and AMS ^{14}C dating

Xiaomei Nian[a,*], Weiguo Zhang[a], Zhanghua Wang[a], Qianli Sun[a], Jing Chen[a], Zhongyuan Chen[a], Simon M. Hutchinson[b]

[a] State Key Laboratory of Estuarine and Coastal Research, East China Normal University, Shanghai 200062, China
[b] School of Environment and Life Sciences, University of Salford, Gt. Manchester M6 6PU, UK

ARTICLE INFO

Editor: Edward Anthony

Keywords:
Luminescence dating
Sediment accumulations rates
Deltaic deposits
The Yangtze River delta

ABSTRACT

Optically stimulated luminescence (OSL) dating has gained increased use in dating deltatic deposits, however, its application can be hindered by the problem of incomplete bleaching. To address this limitation, we test the single-grain OSL method for the first time in the Yangtze River delta. A total of eight OSL and 14 AMS ^{14}C samples were obtained from a 50.8 m long sediment core from the incised valley of the delta. Quartz extracted from eight OSL samples from the core was first measured with small multi-grain aliquots using medium- (45–63 μm) and coarse-grained (90–125 μm or 150–180 μm) fractions to test the internal consistency of their respective ages. The results showed that four of five medium-grained quartz samples appeared to be well bleached. In contrast, the coarse-grained quartz samples revealed poor bleaching, except for two samples from the delta front facies. Five coarse-grained quartz OSL samples were further analyzed using a single-grain OSL technique. Only 0.5–0.7% of the grains passed the rejection criteria. Single-grain OSL dating is appropriate for age determination of coarse-grained sediments which have been affected by incomplete bleaching. However, it consumes a lot of instrument time. Central and minimum age models (CAM and MAM) were used to calculate the burial age of the samples; MAM ages fit best in the stratigraphic sequence. Small aliquots are recommended as effective in identifying incomplete bleaching for medium- or coarse-grained quartz. A comparison of AMS ^{14}C dates and OSL ages shows that ^{14}C values are 1–3 ka older than OSL ages. According to the OSL ages, core SD experienced rapid accumulation 10–8 ka and in the last 2 ka. The former is linked to rapid sea-level rise in early Holocene, while the latter is primarily due to the migration of depo-center towards the core site, rather than entirely increased sediment delivery caused by human activities.

1. Introduction

The Yangtze River delta is formed by the third largest river in the world. It has not only been home to Neolithic civilization in eastern China, but is also the present economic center of the country. Therefore, the delta's evolution and its response to climate, sea-level changes and human activities have been research hotspots for a number of years (e.g. Yan and Xu, 1987; Chen et al., 1988; Chen and Stanley, 1998; Hori et al., 2001, 2002; Wang et al., 2012, 2013; Song et al., 2013; Feng et al., 2016). The main part of the delta is developed from the infill of an incised valley of the paleo-Yangtze River, which was formed during the last glacial stage. The sedimentary sequence of this incised valley has a maximum depth of 80 m, which generally consists of fluvial, estuarine, marine and deltaic facies in an upward ascending order and deposited since the Late Pleistocene (e.g. Li et al., 2000). It provides an opportunity to investigate the geomorphologic evolution and history of land-ocean interaction in the Yangtze River delta through the Holocene. Based on the earlier studies published since the 1970s, a general framework of the Yangtze delta evolution has been proposed and the history coastline changes over the last 8000 years have also been established (Delta Research Group, 1978; Wang et al., 1981). However, limited dating data hinders the detailed examination of the delta's environmental change and its response to global climate and sea-level change. Recently a number of cores (Fig. 1) have been collected from the incised valley and densely dated via the ^{14}C method (e.g. Hori et al., 2001, 2002; Wang et al., 2012, 2013; Song et al., 2013). On the basis of these dates, sediment accumulation rates and relative sea-level change have been discussed.

However, there remain several problems with the ^{14}C method. Among these concerns are the so-called reservoir effects which are

* Corresponding author.
E-mail address: xmnian@sklec.ecnu.edu.cn (X. Nian).

https://doi.org/10.1016/j.margeo.2017.11.008
Received 5 June 2017; Received in revised form 4 November 2017; Accepted 11 November 2017
Available online 15 November 2017

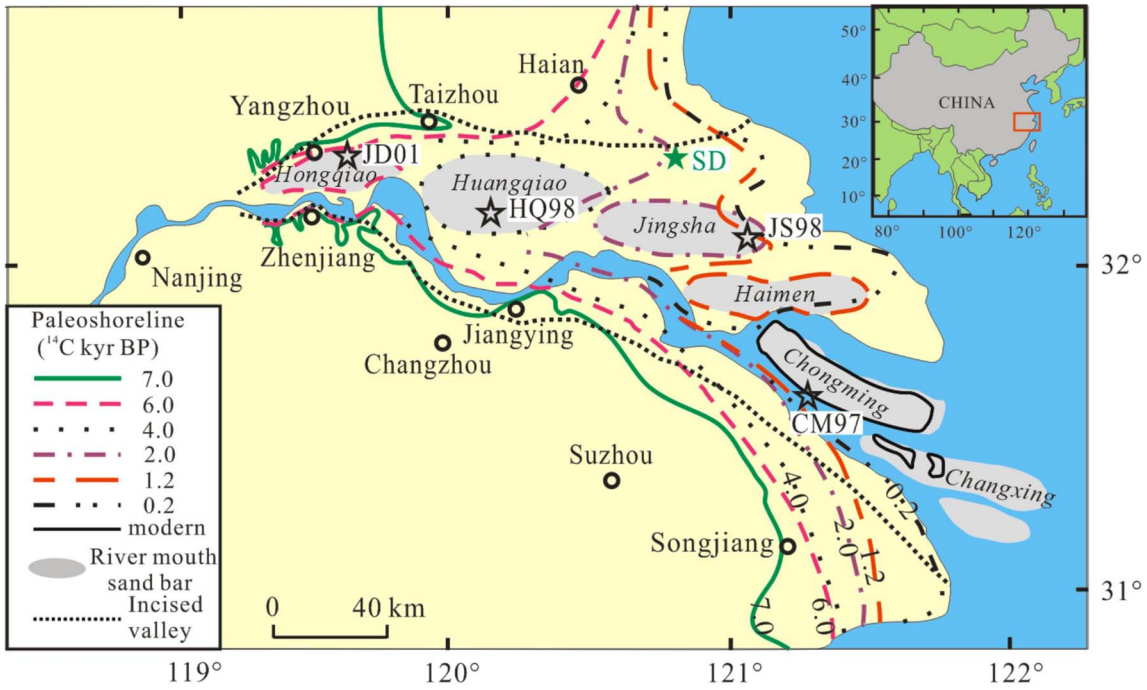

Fig. 1. Location of the SD (Shuangdian) core in the Yangtze River delta, China (modified from Song et al., 2013). Open five-pointed star: cores JD01, HQ98, JS98 and CM97 mentioned in the text (Hori et al., 2001, 2002; Song et al., 2013).

common in coastal environment deposits (e.g. Stanley and Chen, 2000; Marwick et al., 2015). Organic or inorganic carbon may be reworked, which can yield erratic ages. In addition, a paucity of sufficient and suitable material for radiocarbon dating limits the technique's application, particularly in deltaic deposits with coarse sands and negligible organic carbon (e.g. Wang and Li, 2007; Li et al., 2012). Therefore, attempts to decipher the chronology of such Holocene deposits through radiocarbon dating have been hindered.

The optically stimulated luminescence (OSL) dating technique has been developed as an alternative method for Quaternary deposits of various ages (Huntley et al., 1985; Aitken, 1998). With the development of the OSL technique, great improvements in the applicability and precision of luminescence dating have been achieved; especially the modified single-aliquot regenerative-dose (SAR) procedure (Murray and Wintle, 2000) which has been applied to quartz to determine the depositional ages of sediments. OSL use in coastal and marine environment has increased in recent years. In estuarine and delta sediments, OSL dating has been reported by a number of researchers (e.g. Madsen et al., 2005, 2007; Shen and Mauz, 2012; Tamura et al., 2012; Kim et al., 2015; Shen et al., 2015; Sugisaki et al., 2015; Wang et al., 2015; Yang et al., 2015; Gao et al., 2016, 2017). They have found that the OSL method provides generally reliable ages in the study area.

However, these studies have also identified the problem of incomplete bleaching of the OSL signal, which is caused by the attenuation of the solar spectrum in the water environment (e.g. Wallinga, 2002). Previous OSL experiments using the SAR procedure found that quartz of different grain sizes had a different bleaching history, with finer grains being better bleached. The small multiple-grain aliquot and single grain method provide the possibility of identifying poorly/partially bleached grains (e.g. Olley et al., 1999; Duller et al., 2003; Duller, 2008). However, a single grain approach has not been tested in the study area.

The purpose of this paper is two-fold. First, we discuss, for the first time, the robustness of the single-grain optical dating technique for sediments from the Yangtze River delta. Both medium-grained (45–63 μm) and coarse-grained (90–125 μm or 150–180 μm) quartz was used to determine the OSL ages of samples. A special focus of this study is placed on an examination of the OSL ages obtained using both single and multiple grains of quartz, and the comparison of OSL and ^{14}C ages. The degree of sediment bleaching, and the precision and accuracy of optical dating ages in the Yangtze River delta's incised valley are explored. Second, in light of the chronology we derive, and its comparison with previous results, we review the sediment accumulation history of the incised valley.

2. Study area and method

The Yangtze River delta has formed since ~8000 years ago when sea-level was close to the present level and sea-level rise rates slowed down (e.g. Yan and Xu, 1987; Chen and Stanley, 1998; Hori et al., 2001, 2002; Song et al., 2013). During the late Pleistocene, when the sea-level was ca. 120 m below the present, an incised valley was formed, with a maximum depth of 80 m (Li et al., 2000). The incised valley is a funnel shaped trough with its apex located between Zhenjiang and Yangzhou city (Fig. 1). In the incised valley, the sediment sequence comprises a lower, coarse-grained fluvial facies, and an intermediate estuarine and marine facies with coarsening delta facies uppermost. Six sand bodies near the surface (about 20 m in thickness) have been identified and are regarded as river mouth bar deposits formed during the progradation of the delta (e.g. Delta Research Group, 1978; Wang et al., 1981) (Fig. 1).

In this study a 50.8 m long sediment core collected from Shuangdian (SD) was used (Fig. 1). The core location (32°20.3′N, 120°46.75′E; 4.87 m asl) is almost at the northern edge of the incised valley of the lower Yangtze River delta. According to its lithology and stratigraphic correlation with the well-established sedimentary facies in the study area (cores of HQ98 and JS 98 from Hori et al., 2001, 2002), the core covers the deposition history of the entire Holocene epoch and exhibits five sediment units from bottom to top: river channel (U1), tidal sand ridge (U2), prodelta (U3), delta front (U4) and delta plain (U5) (Fig. 2).

3. Sample collection, analytical facilities and protocols

In this study, eight OSL samples and fourteen ^{14}C samples were collected and analyzed to establish a chronological framework for the SD core. Detailed information about the OSL samples is shown in Table 1. In order to understand the grain size distribution of the OSL

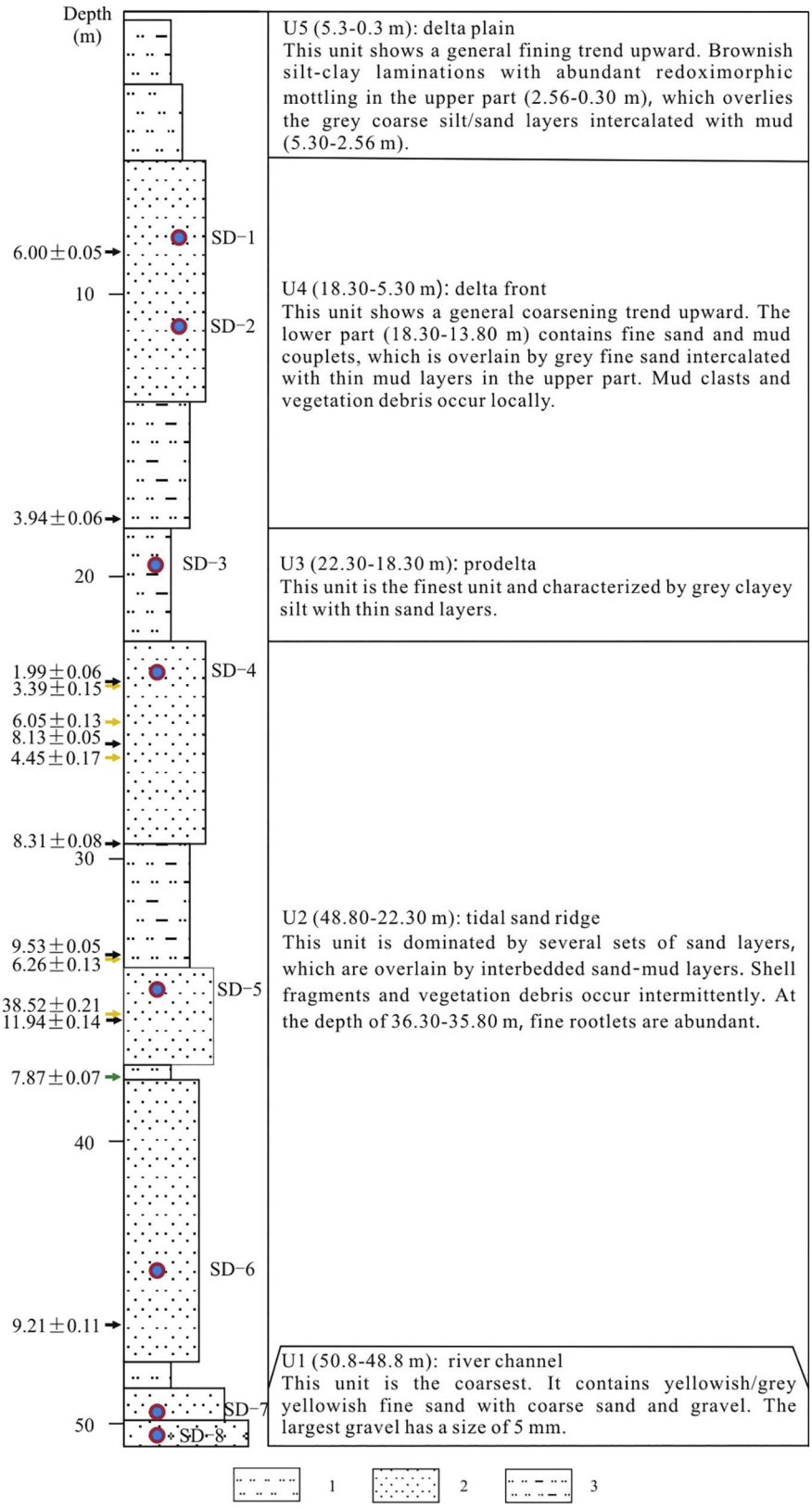

Fig. 2. Lithological description of the SD core showing the OSL sampling site and ^{14}C ages. The ^{14}C ages were converted to ka relative to 2013 CE. Closed circles: OSL sample locations; black arrows: plant fragment samples locations; yellow arrows: shell sample locations; green arrow: peat sample location. 1. Silt; 2. Sand; 3. Silt with thin sand/silt/clay layers or lenses. (For interpretation of the references to color in this figure legend, the reader is referred to the web version of this article.)

samples, their particle size distributions were analyzed by a LS13320 laser diffraction particle size analyzer (Beckman-Coulter, USA). Particle size distribution data are shown in Fig. S1 and these sediments are dominated by sand and silt particle-size fractions. The results indicate that the mode size ranges from 100 to 200 μm, except for samples SD-3 and SD-8 with major peaks around 30–50 μm and 200 μm, respectively. Consequently, medium-grained (45–63 μm) and coarse-grained quartz (90–125 μm or 150–180 μm) fractions were extracted from the sediments for optical dating.

OSL sample preparation and measurement were carried out under subdued red light conditions. In the laboratory, the samples were removed from the sediment core in metal tubes and kept in a refrigerator

Table 1
OSL sample code, radionuclide concentrations, depth, water content and dose rates of the samples from the SD core.

Field code	Lab code	U (ppm)	Th (ppm)	K (%)	Depth (m)	Water (%)	Grain size (μm)	Environmental dose rate (Gy/ka)				
								Alpha	Beta	Gamma	Cosmic	[a]Total
SD-1	L58	1.50 ± 0.07	9.98 ± 0.29	1.71 ± 0.05	8.15–8.30	27 ± 5	45–63	0.10 ± 0.04	1.32 ± 0.07	0.81 ± 0.04	0.079 ± 0.008	2.34 ± 0.09
							90–125	–	1.26 ± 0.07			2.15 ± 0.08
SD-2	L5	1.66 ± 0.08	8.79 ± 0.26	1.83 ± 0.06	11.15–11.3	33 ± 5	45–63	0.09 ± 0.04	1.31 ± 0.07	0.76 ± 0.04	0.060 ± 0.006	2.25 ± 0.09
							90–125	–	1.25 ± 0.07			2.08 ± 0.08
SD-3	L59	1.44 ± 0.07	10.10 ± 0.28	1.52 ± 0.05	19.15–19.3	33 ± 5	45–63	0.09 ± 0.04	1.14 ± 0.06	0.74 ± 0.03	0.033 ± 0.003	2.03 ± 0.08
							90–125	–	1.09 ± 0.06			1.89 ± 0.07
SD-4	L6	3.56 ± 0.12	8.98 ± 0.27	1.85 ± 0.06	23.15–23.3	35 ± 5	45–63	0.13 ± 0.05	1.48 ± 0.07	0.91 ± 0.04	0.025 ± 0.003	2.58 ± 0.10
							90–125	–	1.41 ± 0.07			2.35 ± 0.08
SD-5	L60	0.94 ± 0.05	5.72 ± 0.20	1.76 ± 0.06	34.15–34.3	34 ± 5	45–63	0.06 ± 0.02	1.14 ± 0.06	0.58 ± 0.03	0.014 ± 0.001	1.82 ± 0.07
							90–125	–	1.10 ± 0.06			1.72 ± 0.07
SD-6	L61	1.25 ± 0.06	8.26 ± 0.25	1.52 ± 0.05	44.65–44.80	33 ± 5	45–63	0.08 ± 0.03	1.09 ± 0.06	0.66 ± 0.03	0.009 ± 0.001	1.87 ± 0.08
							90–125	–	1.04 ± 0.06			1.74 ± 0.07
SD-7	L62	1.63 ± 0.07	8.67 ± 0.26	1.90 ± 0.06	49.65–49.80	36 ± 5	45–63	0.09 ± 0.03	1.31 ± 0.07	0.75 ± 0.03	0.008 ± 0.001	2.18 ± 0.08
							90–125	–	1.25 ± 0.06			2.04 ± 0.08
SD-8	L63	0.99 ± 0.05	9.77 ± 0.28	1.57 ± 0.05	50.65–50.80	34 ± 5	45–63	0.08 ± 0.03	1.11 ± 0.06	0.69 ± 0.03	0.007 ± 0.001	1.92 ± 0.08
							150–180	–	1.03 ± 0.06			1.76 ± 0.07

[a] Includes an alpha internal dose rate of 0.03 ± 0.02 Gy/ka.

to ensure limited evaporation. After removing the light-exposed portion of the sample from both ends of the metal tubes, the non-light-exposed sediment from their inner section was treated with HCl and H_2O_2 to remove any carbonates and organics, respectively. Samples were then sieved in to the selected grain size fractions (45–63 μm, 90–125 μm or 150–180 μm). The medium-grained size and the coarse-grained size fraction were etched with 30% H_2SiF_6 for 3–4 days and 40% HF for 40 min, respectively, and then washed with HCl and water to isolate the quartz grains. The purity of the isolated quartz was checked by infrared-stimulated luminescence measurements to ensure no feldspar contamination was present in any of the samples (Duller, 2003).

OSL measurements were performed using an automated Risø TL/OSL-DA-20 reader (Bøtter-Jensen et al., 2003) equipped with a calibrated beta ($^{90}Sr/^{90}Y$) source with an EMI 9235 QA photomultiplier tube (PMT). Blue light-emitting diodes (90% power) emitting light at 470 nm with a total power of 97 mW/cm^2 were used for single aliquot quartz measurements. The green laser (90% power, 532 nm, 100 mW/cm^2) was used for quartz single-grain measurements. 7.5 mm Hoya U-340 filters were used for signal detection. Separated quartz grains were mounted on 9.7 mm diameter aluminum discs for the multiple-grain single aliquot analyzes using silicone oil and loaded on to single-grain discs with an array of 10 by 10 holes, each 300 μm in depth and diameter.

Multiple-grain and single-grain measurements were used to determine the equivalent-dose (D_e) of these samples using the single-aliquot regenerative-dose (SAR) protocol (Murray and Wintle, 2000). A 200 °C preheat of 10 s and a 160 °C cut heat of 0 s were applied to all dose measurements on the basis of preheat plateau tests. For the multiple-grain aliquots (2 mm in diameter), stimulation with blue LEDs at 125 °C for 40 s was employed and to ensure the removal of any remaining signal a blue light stimulation at 280 °C for 40 s was applied at the end of each cycle. For single-grain measurements, the OSL was stimulated from each grain in turn by the green laser at 125 °C for 0.9 s. The first 0.4 s of stimulation, minus a background derived from the last 10 s of stimulation, was used for the multiple-grain aliquots, while the first 0.17 s of the signals, minus a background evaluated from the average signal in the last 0.255 s, was used for single grain D_e calculation. All the regeneration data were fitted using a single saturating exponential for the interpolation of D_e.

In this study, neutron activation analysis (NAA) was used to determine the uranium (U), thorium (Th) and potassium (K) contents of the samples (Table 1). An alpha-efficiency (a-value) of 0.04 ± 0.02 was used to estimate the dose rate of the 45–63 μm quartz grains (Rees-Jones, 1995). The measured moisture contents were used, allowing ± 5%, for each value in the age calculations. An alpha internal dose rate of 0.03 ± 0.02 Gy/ka was assumed for quartz samples. Environmental dose-rates and final age calculations were made using the 'DRAC' program developed by Durcan et al. (2015). The dose-rate conversion factors of Adamiec and Aitken (1998), alpha-attenuation factors of Brennan et al. (1991), beta-attenuation factors of Guerin et al. (2012) and cosmic dose rates from Prescott and Hutton (1994) were used to calculate the dose rate.

The 14 AMS^{14}C samples were analyzed by Beta Analytic Radiocarbon Dating Laboratory (Florida, USA). Calibrated ages were calculated using the CALIB REV 7.1 program, the IntCal13 Marine13 (shell) and IntCal13 (plant fragment, peat) calibration curve of Reimer et al., 2013. In the following discussion, we use the median age of the two-sigma calibrated radiocarbon dates. −1 ± 143 years regional marine reservoir effect (ΔR) was applied to the shell samples (Southon et al., 2002; Kong and Lee, 2005; Yoneda et al., 2007). The ^{14}C ages were converted to ka relative to 2013 CE for comparison to the OSL ages.

Table 2
Properties, $\delta^{13}C$ values, conventional and calibrated ^{14}C ages of samples from the SD core.

Lab number	Depth (m)	$\delta^{13}C$ (‰)	Material	Conventional age (a BP)	Calibrated age (a BP, 2σ)	ka (relative to 2013 CE)
Beta-383507	8.5	− 24.8	Plant fragments	5160 ± 30	5890–5990	6.00 ± 0.05
Beta-381415	17.96	− 27.1		3570 ± 30	3825–3935	3.94 ± 0.06
Beta-383508	23.86	− 28.1		1970 ± 30	1865–1995	1.99 ± 0.06
Beta-379308	23.87	− 10.5	Shell	3470 ± 30	2950–3700	3.39 ± 0.15
Beta-381417	25.15	− 5.9		5610 ± 30	5665–6300	6.05 ± 0.13
Beta-381418	25.92	− 25.1	Plant fragments	7230 ± 30	7970–8160	8.13 ± 0.05
Beta-381419	26.4	− 10	Shell	4260 ± 30	3980–4785	4.45 ± 0.17
Beta-381420	29.48	− 27	Plant fragments	7390 ± 30	8165–8325	8.31 ± 0.08
Beta-383509	33.5	− 28.6		8430 ± 30	9420–9520	9.53 ± 0.05
Beta-379309	33.55	− 7.8	Shell	5790 ± 30	5880–6520	6.26 ± 0.13
Beta-379310	35.6	− 8.1		34,450 ± 30	38,242–38,667	38.52 ± 0.21
Beta-381422	35.85	− 23.6	Plant fragments	10,180 ± 30	11,705–12,055	11.94 ± 0.14
Beta-381423	37.68	− 25	Peat	6990 ± 30	7735–7875	7.87 ± 0.07
Beta-381424	46.5	− 25.8	Plant fragments	8190 ± 30	9030–9255	9.21 ± 0.11

4. Results

4.1. AMS ^{14}C dating results

Sample information and AMS^{14}C dating results are shown in Table 2 and Fig. 2. The ^{14}C ages showed that the core ranges in age from 1.99 ka to 38.52 ka. The ^{14}C age variations are not always in stratigraphic order and age reversals are common in the core. In addition, ages derived from shell and plant fragments fail to match.

4.2. Luminescence dating results

4.2.1. The SAR protocol for multiple grains

In order to test the effects of preheat conditions for D_e estimation, preheat plateau tests were carried out on both the 45–63 μm and 90–125 μm sizes of quartz sample SD-3 between 160 °C and 300 °C in 20 °C steps with a test dose of 1.01 Gy. Preheat plateaus for the sample indicated no dependence of dose for preheat temperatures between 160 and 220 °C with a fixed cut-heat of 160 °C using at least six aliquots, respectively (Fig. S2a and b). Ratios of given to recovered dose as a function of preheat temperature are shown in Fig. S2c and d. The ratios were found to be indistinguishable for 10 s preheats between 180 and 260 °C for 45–63 μm quartz and between 160 and 220 °C for 90–125 μm quartz. Taken together, a preheat of 10 s at 200 °C and a cut heat of 0 s at 160 °C were selected for D_e determination based on preheat plateau.

Sensitivity changes were monitored by repeated measurement of the OSL signal in response to a fixed regenerative dose 3.64 Gy versus a fixed test dose 1.01 Gy (Murray and Wintle, 2000). A linear relationship between regenerative dose and test dose OSL signals was found (Fig. S3, a), indicating that the OSL test dose signals correlate well with the regeneration OSL signals of the SAR protocol.

To further test the suitability of the SAR protocol, dose recovery test was applied to all the core samples (Murray and Wintle, 2003). In the experiment, previously SOL2-bleached aliquots (1 h) were given a beta dose (approximately equal to the natural dose) in the instrument, and then the OSL signals from each aliquot were measured with a small fixed test dose. The mean ratio of the recovered dose to the given dose were between 0.91 ± 0.06 and 1.07 ± 0.10 for medium- and coarse-grained quartz samples, respectively (Table S1). The results of the above experiments demonstrate that the SAR protocol is suitable for the sediments under investigation.

Typical natural OSL decay curves and SAR growth curves for quartz sample SD-3 are shown in Fig. 3. The analyzed OSL signals displayed a rapid decay in the case of both medium- and coarse-grained quartz fractions. The recycling ratio and recuperation were used to monitor the aliquots contributing to D_e determination using the SAR protocol. The recycling ratios lying within 0.9–1.1 and recuperation of < 5% were chosen as rejection criteria. In these experiments, the SAR protocol was used to determine the burial dose of the samples, in which preheat and cut-heat temperatures were fixed at 200 °C for 10 s and 160 °C for 0 s, respectively.

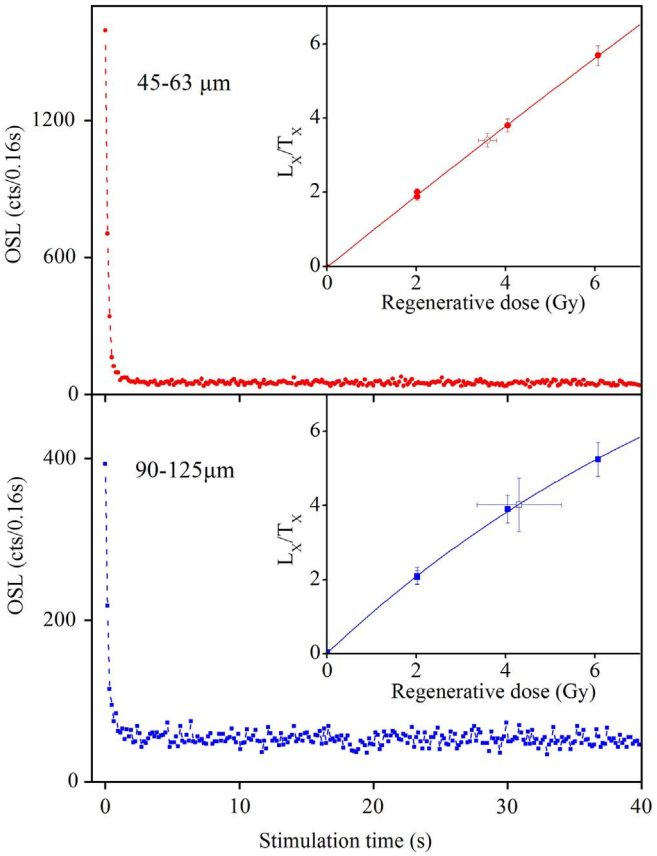

Fig. 3. Natural OSL decay curves for 45–63 μm and 90–125 μm quartz from sample SD-3; the inset figures show the corresponding sensitivity-corrected growth curves using the SAR protocol. Solid symbols: regenerative and repeated doses; hollow (outline) symbols: natural dose.

Sixteen to forty-two aliquots were used for each grain size fraction of the core samples in order to obtain the D_e values, with the exception of the 45–63 μm fractions of samples SD-5, SD-7 and SD-8, which did not yield enough material of this size fraction for analysis. The D_e estimates for two representative samples, SD-3 and SD-6, are shown in the radial plots in Fig. 4, and dose measurements for the other samples are plotted in Fig. S4 (medium-grained quartz) and Fig. S5 (coarse-grained

quartz). For medium-grained quartz, the D_e distributions are symmetrical except for sample SD-6. Their over-dispersion (OD) values were between 5% and 13% (with an average value of 8%) for samples SD-1 to SD-4, which was similar in magnitude to that observed previously for the dose recovery measurements (ca. 10%), and 23% for sample SD-6. For coarse-grained quartz, except for samples SD-1 and SD-2 (with an OD value of 15% and 19%), the other six samples were all asymmetrical with an OD varying from 16% to 47% (with an average value of 30%), which is higher than the values obtained from the dose recovery measurements (ca. 10%). The above data lead us to believe that the coarse-grained quartz samples have the potential problem of incompletely bleaching at deposition. The OD values for medium-grained quartz are smaller than those for the coarse-grained quartz. However, according to Duller (2008), we can estimate the number of grains with the fixed grain-size interval and aliquot size using R. For medium-grained (45–63 μm) and coarse-grained (90–125 and 150–180 μm) quartz, the number of grains mounted on the 2-mm aliquots are ca. 892, 225 and 96, respectively. The number of grains shows that the small OD values for the medium-grained quartz are very likely to have been induced by the more significant signal averaging effect than the coarse-grained quartz. Therefore more evidence is needed to know whether the medium component was better bleached. The D_e values and OSL ages were obtained from the central age model (CAM) and the minimum age model (MAM) (Galbraith et al., 1999). A 10% OD was used for multi-grain aliquots (derived from unpublished data of samples from the same region). The results are summarized in Table 3.

The CAM ages of medium-grained quartz for samples SD-1, SD-2, SD-3 and SD-4 were indistinguishable from those of MAM ages ranging from ca. 1.54 ka to 2.18 ka in the correct stratigraphic order However, the MAM age of sample SD-6 was ca. 8.46 ka, while the age determined by CAM was slightly higher. For coarse-grained quartz, the CAM and MAM ages of samples varied from ca. 1.65 to ca. 82 and ca. 1.58 to ca. 62 ka (Table 2). The samples presented systematically higher CAM ages for coarse-grained quartz than corresponding ages of medium-grained quartz, apart from samples SD-1 and SD-2 from mouth bar sediments (U6). The CAM or MAM ages of these two coarse-grained quartz samples (samples SD-1 and SD-2) are similar to the corresponding medium-grained quartz ages within the experimental errors, indicating that incomplete bleaching is probably not important for these two samples. The coarse-grained samples for samples SD-3 to SD-8 revealed incomplete bleaching as discussed above. Here we consider the likelihood of partial bleaching of coarse-grained quartz, MAM ages of the samples are considered to be more accurate of the depositional ages, and are similar to the values of medium-grained quartz CAM (except for SD-6) or MAM ages. Thus, the MAM ages were adopted in the following discussion.

4.2.2. The SAR protocol for single grains

To overcome the incomplete bleaching problem in coarse-grained quartz, the single-grain optical dating method was applied to the five samples to identify well-bleached grains (One sample was not available due to the insufficient quantity of material.) The spread of D_e observed for coarse-grained quartz using multiple-grain aliquots suggests that partial resetting, because of heterogeneous light exposure at the time of deposition, may be an issue for luminescence dating of some samples. Here single-grain optical dating was used to examine the extent of heterogeneous bleaching of coarse-grained quartz extracted from samples SD-3, SD-5 to SD-8 of the SD core. The D_e values obtained from single grain measurements were analyzed using CAM and MAM to constrain the true burial doses and ages. The expected OD value was set to 20% for single grains (Cunningham et al., 2011).

The OSL signal from each individual grain was not uniform, the single-grain data were screened according to the following standard rejection criteria: (1) a natural test dose (Tn) signal > 3 sigma above BG, (2) a maximum test dose error < 20%, (3) a maximum recuperation ratio < 5%, (4) a recycling ratio falling inside the range of 0.9–1.1, (5) a sensitivity corrected natural luminescence intensity (L_N/T_N) lower than the regenerated saturation level, (6) the IR depletion ratio (Duller, 2003) within 10% of the unity. Single-grain measurements showed that the samples have a relatively dim OSL signal, with only about 0.9–3.7%

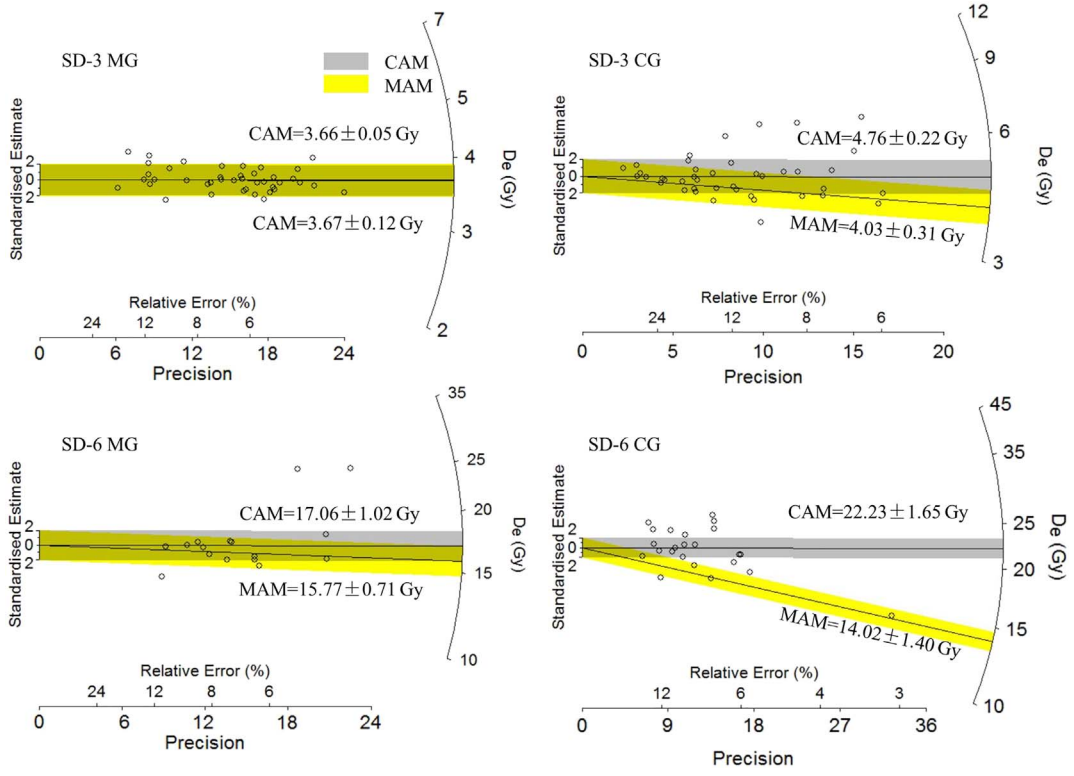

Fig. 4. Radial plots showing the distribution of equivalent doses of aliquots of 45–63 μm and 90–125 μm quartz from representative samples SD-3 and SD-6.

Table 3
Summary of D_e values and OSL age estimates for medium- and coarse-grained quartz extracted from SD core samples using the central age model (CAM) and the minimum age model (MAM). OSL ages are relative to 2013 CE.

Field no.	Medium-grained quartz						Coarse-grained quartz					
	Number of aliquots	Over-dispersion	CAM-D_e (Gy)	CAM-Age (ka)	MAM-D_e (Gy)	MAM-Age (Gy)	Number of aliquots	Over-dispersion	CAM-D_e (Gy)	CAM-Age (ka)	MAM-D_e (Gy)	MAM-Age (ka)
SD-1	23	0.07 ± 0.02	3.62 ± 0.08	1.55 ± 0.07	3.61 ± 0.18	1.54 ± 0.10	19	0.15 ± 0.04	3.60 ± 0.15	1.65 ± 0.09	3.65 ± 0.20	1.68 ± 0.11
SD-2	27	0.05 ± 0.02	3.56 ± 0.06	1.58 ± 0.07	3.56 ± 0.08	1.58 ± 0.07	35	0.19 ± 0.03	3.57 ± 0.14	1.70 ± 0.09	3.32 ± 0.21	1.58 ± 0.12
SD-3	42	0.06 ± 0.01	3.66 ± 0.05	1.80 ± 0.08	3.67 ± 0.12	1.81 ± 0.09	41	0.25 ± 0.04	4.76 ± 0.22	2.52 ± 0.15	4.03 ± 0.31	2.14 ± 0.18
SD-4	18	0.13 ± 0.03	5.61 ± 0.20	2.18 ± 0.11	5.04 ± 0.36	1.96 ± 0.16	26	0.16 ± 0.03	5.09 ± 0.20	2.14 ± 0.11	4.41 ± 0.36	1.86 ± 0.17
SD-5	—	—	—	—	—	—	21	0.25 ± 0.06	20.73 ± 1.31	12.04 ± 0.89	15.89 ± 1.43	9.23 ± 0.91
SD-6	16	0.23 ± 0.04	17.06 ± 1.02	9.15 ± 0.66	15.77 ± 0.71	8.46 ± 0.51	23	0.34 ± 0.05	22.23 ± 1.65	12.78 ± 1.07	14.02 ± 1.40	8.06 ± 0.86
SD-7	—	—	—	—	—	—	23	0.47 ± 0.07	35.16 ± 3.51	17.23 ± 1.83	19.09 ± 1.64	9.36 ± 0.87
SD-8	—	—	—	—	—	—	17	0.33 ± 0.06	144 ± 10	82 ± 7	109 ± 10	62 ± 6

Note: "—" indicates samples (SD-5, 7, 8) lacking enough quartz for OSL measurement in the 45–63 μm grain size fraction.

of the grains having sufficient signal to build the growth curves. Grains which passed the above rejection criteria and were chosen to determine the D_e value account for only 0.51–0.73% of the total quartz grains (Table 4).

Representative OSL decay curves and dose-response curves of sample SD-3 and SD-6, shown in Fig. 5 display the greatest variability observed. Table 3 shows the single-grain optical dating results. The single-grain D_e estimates for representative samples SD-3 and SD-7 are presented as radial plots in Fig. 6 and the D_e estimates for other samples are plotted in Fig. S6. The OD varied among these five samples range between ca. 15% and ca. 79%. The OD for samples SD-5 and SD-6 in the resultant quartz single-grain dose distributions are smaller than 20% and their ages obtained using the CAM, within experimental error, were consistent with the ages using the MAM. For the samples SD-3, SD-7 and SD-8, there are large differences between the central and minimum ages (25–145%) determined using the single-grain SAR protocol. High OD for the D_e distributions from the single-grain measurements confirms that there may be a mixture of grains with different bleaching histories in some of the samples. The single-grain data analyzed using MAM are in stratigraphic order.

5. Discussion

5.1. OSL chronology

The multiple-grain, single-aliquot OSL dating method indicates that medium-grained quartz is better bleached than coarse-grained quartz. For the former, four of five medium-grained quartz samples were well bleached at the time of deposition. These samples come from delta front (U4), prodelta (U3) and tidal sand ridge (U2) facies. On the other hand, six of eight samples exhibited incomplete bleaching for coarse-grained quartz, except for two samples from the delta front (U4). According to grain-size analysis in the present Yangtze River estuary, suspended sediment is composed mainly of fine silt and clay, whereas bed sediment is composed of sand (Table 5) (Wang et al., 1997). Such relatively fine suspended grains are expected to be exposed to sunlight more than coarse bed-load grains during transportation, hence, the former is likely to be better bleached than the latter. As a result, medium-grained quartz from suspended sediments is generally better bleached than coarse-grained quartz transported as bed sediments.

However, when there is insufficient medium or fine-grained quartz in sand-dominated sequences for dating, we have to rely on the coarse grain-size fraction. Although partial bleaching is a significant problem for some coarse-grain sediments, small-aliquot or single-grain OSL technique can help to identify light-safe grains, and therefore facilitate the use of coarse-grain for dating.

The single-grain method provides a means of overcoming the problem of incomplete bleaching in coarse-grained quartz. Our results found that a very small percentage (< 0.8%) of quartz grains were bright enough to produce regenerated growth curves to determine the D_e values (Table 3). The single-grain ages were statistically indistinguishable from those obtained from the multi-grain dating method for coarse-grained quartz using the CAM due to the small proportion of grains suitable for OSL dating. However, the single-grain method is time consuming.

Our results show that MAM ages are more reliable for both multi-grain and single-grain OSL measurements, since these ages are in accordance with the stratigraphically sequence of the core. Furthermore, MAM ages are much closer to AMS ^{14}C ages at certain depths.

5.2. Comparison of OSL and ^{14}C dating results

Six of the fourteen ^{14}C dates from the SD core in the Yangtze River delta fall within the expected range of OSL dating. Some samples gave too old AMS ^{14}C ages; some 1 ka to 30 ka older than the OSL dates. For instance, two samples from almost 35 m in depth showed greatly

Table 4
Summary of grains passing the rejection criteria, D_e statistics and age model results of samples SD-3 and SD-5 to SD-8.

Sample no.	SD-3	SD-5	SD-6	SD-7	SD-8
Grain size (μm)	90–125	90–125	90–125	90–125	150–180
Total number of grains measured	8200	5100	6500	5300	5800
Gains with a signal	145	376	317	1675	328
Grains with growth curves	76	134	121	195	135
Grains with growth curves were rejected if:					
(1) Tn signal < 3*BG	1	8	3	36	2
(2) maximum test dose error > 20%	16	65	51	116	37
(3) Recuperation ratio > 5%	6	12	15	19	34
(4) Recycling ratio > 1.1 or < 0.9	10	26	10	19	15
(5) No Ln/Tn intersection	0	10	11	58	12
(6) IR depletion ratio > 1.1 or < 0.9	9	11	21	15	35
Sum of rejected grains	34	97	88	160	101
Acceptable number of grains	42	37	33	35	34
Proportion of acceptable grains	0.51%	0.73%	0.51%	0.66%	0.59%
Over-dispersion	0.27 ± 0.04	0.15 ± 0.04	0.19 ± 0.04	0.79 ± 0.11	0.24 ± 0.06
CAM D_e (Gy)	4.79 ± 0.25	13.98 ± 0.56	16.09 ± 0.72	45.56 ± 6.45	136 ± 8
CAM age (ka)	2.54 ± 0.16	8.12 ± 0.45	9.25 ± 0.55	22.33 ± 3.26	77 ± 5
MAM D_e (Gy)	3.83 ± 0.46	13.93 ± 1.10	16.07 ± 1.38	18.62 ± 2.75	119 ± 16
MAM age (ka)	2.03 ± 0.26	8.09 ± 0.71	9.24 ± 0.87	9.12 ± 1.39	68 ± 9

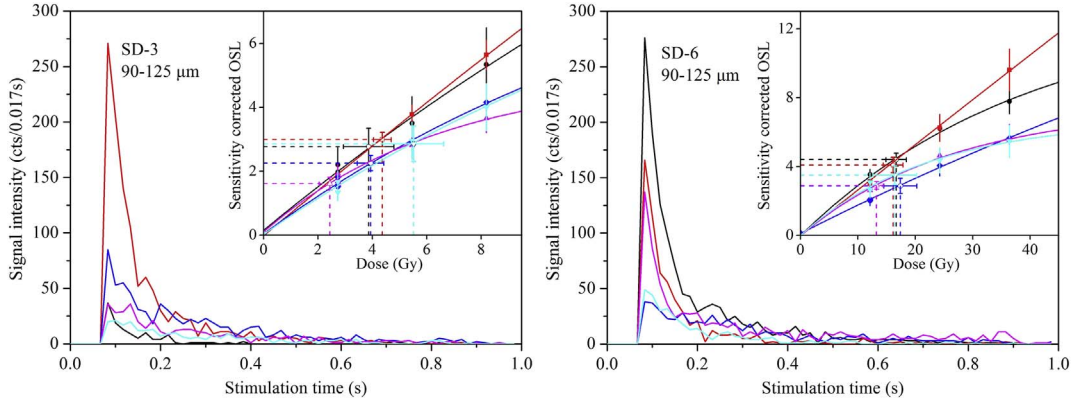

Fig. 5. Representative natural OSL decay curves and dose-response curves (insert) for samples SD-3 and SD-6 obtained with the single-grain SAR protocol. Symbols and lines in different colors represent different grains. (For interpretation of the references to color in this figure legend, the reader is referred to the web version of this article.)

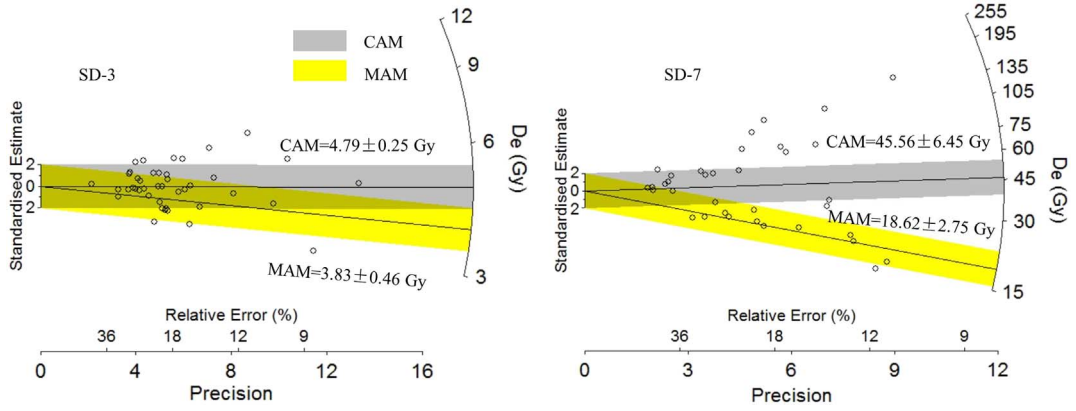

Fig. 6. Radial plots showing the distribution of equivalent doses of single grains from the coarse-grained quartz fractions of representative samples SD-3 and SD-7.

differing dates of ca. 12 ka and 39 ka. Furthermore, ^{14}C age reversals are common (Table 2 and Fig. 7). The inconsistency of ^{14}C ages suggests that they are likely to record disturbances in the sedimentary environment. Stanley and Chen (2000) suggested that the introduction of old carbon during sediment storage and reworking along the dispersal path from the catchment to the coast was the main cause of older dates and age reversals. Therefore, closer attention needs to be paid to the radiocarbon dates of the Holocene sequence of the Yangtze River delta area. A multi-method geochronological approach, such as OSL and ^{14}C dating techniques, would allow for an improved assessment of the uncertainties involved in the reconstruction of the dynamic and complex depositional environments of the river deltas.

5.3. Sediment accumulation rates

The OSL technique appears to provide a better chronology than AMS ^{14}C in the studied core. According to the multiple and single grain MAM OSL ages, a clear three-phase change in sedimentation rate has

Table 5
Grain-size characteristics of modern sediment loads in the Yangtze River (Wang et al., 1997).

	Locality	Sample no.	Grain size parameter		Sand-silt-clay ratios (%)			Sediment categories
			[a]Md (μm)	[b]Mz (μm)	Sand	Silt	Clay	
Suspended sediment	Yichang	C_{X1}	11.8	10.8	18.3	42.7	39	Clayey silt
	Hankuo	C_{X2}	7.3	6.5	11.3	44.7	44	Clayey silt
	Datong	C_{X3}	11.1	9.8	17	39.5	43.5	Silty clay
Bed sediment	Yichang	C_{d1}	233	179	80.5	19.5	0	Sand
	Hankuo	C_{d2}	268	250	92.6	7.4	0	Sand
	Datong	C_{d3}	218	206	91.3	8.7	0	Sand
	Nanjing	C_{d4}	250	200	84	16	0	Sand
	Jiangyin	C_{d5}	5.2	4.7	5.5	42	52.5	Silty clay
	Changjiang Estuary	C_{d6}	4.8	5.6	10.5	19.5	70	Silty clay

[a] Md: median grain size.
[b] Mz: mean grain size.

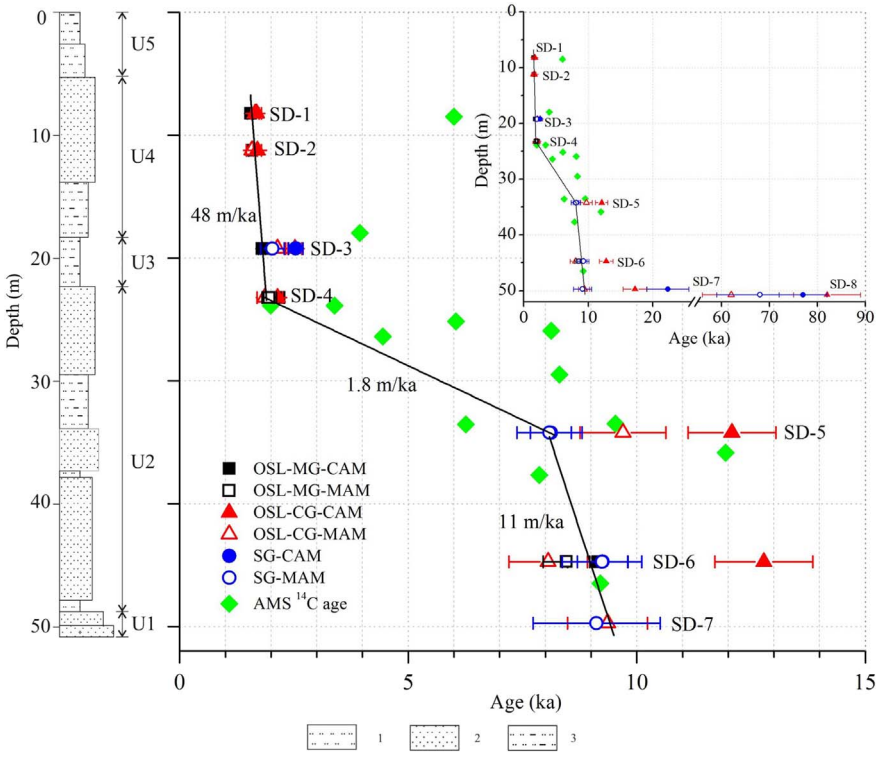

Fig. 7. Lithological profile of the SD core showing the correlation between quartz OSL ages and ^{14}C ages. MG: medium grains; CG: coarse grain; SG: single grain. The main figure shows the ages of the samples during the period 0–15 ka; the inset figure showed the ages of all the samples during the period 0–90 ka.

occurred since ca. 9 ka. A rapid sedimentation rate of ca. 11 m/ka occurred around 9–8 ka, followed by a lower rate of about 1.8 m/ka between 8 ka and 2 ka with the highest accumulation rate of ca. 48 m/ka occurring since 2 ka. An extreme high sedimentation rate during the early Holocene is also evident in other cores in the Yangtze delta and has been linked to the rapid sea-level rise and the large accommodation space for sediment infilling in this period (Hori and Saito, 2007) (Fig. 8). Following a rapid sea-level rise in the early Holocene, the sediment accumulation rate decreased at the SD core site, as a result of the landward retreat of shoreline and migration of the depo-center inland (Hori and Saito, 2007). This is also evident in the cores eastward of SD, i.e., JS98 and CM97. The highest rate of sedimentation since 2 ka is generally interpreted as reflecting the increased human activities in the catchment over the past 2000 years (Liu et al., 2007), which lead to increased sediment delivery. However, this increase may also have been caused by the migration of mouth bar deposition with time. As shown in Fig. 8, each core in the incised valley has a rapid sedimentation rate in the top 20 m, which covers the delta front and delta plain facies. The most landward cores, i.e., JD and HQ98, display rapid deposition during the 6–5 ka period. The nearby cores JS98 and CM97 are similar to core SD in that rapid deposition occurred between 3 and 1 ka. This pattern reflects with eastward delta progradation since 8 ka when sea-level rise slowed down. It highlights that a shift of deposition center should be taken into account when interpreting sediment accumulation rate change in a delta environment.

6. Conclusions

Quartz from sediments from the SD core taken from the incised valley of the Yangtze River delta has been investigated using multiple-grain and single-grain optical dating methods. The results indicate that medium-grained quartz signals were better bleached than coarse-grained quartz. To overcome the bleaching problems in coarse-grained quartz, the SAR protocol for single grains was applied to determine the burial dose. In our samples, only a very small percentage of quartz grains were bright enough for OSL dating. The single-grain age confirms that the multiple-grain age of coarse-grain quartz is reliable, despite the incomplete bleaching problems associated with multiple coarse-grain

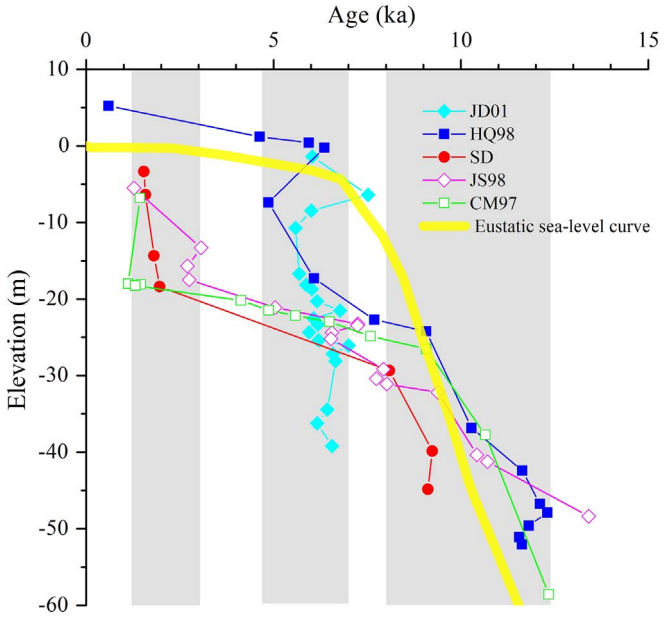

Fig. 8. Age-depth relationships and accumulation curves for cores JD01, HQ98, SD, JS98 and CM97 and a sea-level curve (Lambeck et al., 2014). The grey shaded area: the time period with high accumulation rates.

quartz dating. In summary, both medium- and coarse-grain quartz can be used for dating. The AMS radiocarbon ages of the SD core were ca. 1–30 ka older than the OSL ages due to contamination by old carbon material.

Our OSL chronology of the SD core contributes to a better chronological framework in the Yangtze River delta. It reveals that sediment accumulation rates varied during the Holocene. Rapid deposition between 11 and 8 ka is linked to the rapid rise of sea-level at this time. The subsequent slower deposition between 8 and 2 ka can be linked to the landward shift of delta depocenter. The rapid deposition over the last 2 ka is mostly a reflection of the movement of the depo-center towards the core site due to delta progradation.

Supplementary data to this article can be found online at https://doi.org/10.1016/j.margeo.2017.11.008.

Acknowledgements

We thank the three anonymous reviewers and the editor of the journal whose detailed reviews and suggestions led to many improvements in the manuscript. This research has been supported by the National Natural Science Foundation of China (41771009; 41302135; 41271223), the China Postdoctoral Special Science Foundation (2017T100284), the China Postdoctoral Science Foundation (2015M571521), the State Key Laboratory Special Fund (2014RCDW02, SKLEC-2012KYYW01).

References

Adamiec, G., Aitken, M., 1998. Dose-rate conversion factors: update. Ancient TL 16, 37–50.
Aitken, M.J., 1998. An Introduction to Optical Dating. Oxford University Press, New York.
Bøtter-Jensen, L., Andersen, C.E., Duller, G.A.T., Murray, A.S., 2003. Developments in radiation, stimulation and observation facilities in luminescence measurements. Radiat. Meas. 37, 535–541.
Brennan, B.J., Lyons, R.G., Phillips, S.W., 1991. Attenuation of alpha particle track dose for spherical grains. Int. J. Radiat. Appl. Instrum. Part D Nucl. Tracks Radiat. Meas. 18, 249–253.
Chen, Z.Y., Stanley, D.J., 1998. Rising sea level on eastern China's Yangtze delta. J. Coast. Res. 14, 360–366.
Chen, J.Y., Shen, H.T., Yun, C.X., 1988. Dynamic Processes and Morphological Evolution of Yangtze Estuary. Shanghai Science and Technology Press, Shanghai (In Chinese with English summary).
Cunningham, A., Wallinga, J., Minderhoud, P., 2011. Expectations of scatter in equivalent-dose distributions when using multi-grain aliquots for OSL dating. Geochronometria 38, 424–431.
Delta Research Group, Department of Marine Geology, Tongji University, 1978. Holocene formation and development of the Yangtze Delta. Chin. Sci. Bull. 35 (5), 310–313 (In Chinese).
Duller, G.A.T., 2003. Distinguishing quartz and feldspar in single grain luminescence measurements. Radiat. Meas. 37, 161–165.
Duller, G.A.T., 2008. Single-grain optical dating of quaternary sediments: why aliquot size matters in luminescence dating. Boreas 37, 589–612.
Duller, G.A.T., Bøtter-Jensen, L., Murray, A.S., 2003. Combining infrared- and green-laser stimulation sources in single-grain luminescence measurements of feldspar and quartz. Radiat. Meas. 37, 543–550.
Durcan, J.A., King, G.E., Duller, G.A.T., 2015. DRAC: dose rate and age calculation for trapped charge dating. Quat. Geochronol. 28, 54–61(DRAC_1.1, www.aber.ac.uk/alrl/drac).
Feng, Z.B., Liu, B.H., Zhao, Y.X., Li, X.S., Jiang, L., Si, S.K., 2016. Spatial and temporal variations and controlling factors of sediment accumulation in the Yangtze River estuary and its adjacent sea area in the Holocene, especially in the Early Holocene. Cont. Shelf Res. 125, 1–17.
Galbraith, R.F., Roberts, R.G., Laslett, G.M., Yoshida, H., Olley, J.M., 1999. Optical dating of single and multiple grains of quartz from Jinmium rock shelter, Northern Australia: part 1, experimental details and statistical models. Archaeometry 41, 339–364.
Gao, L., Long, H., Shen, J., Yu, G., Yin, Y., 2016. High-resolution OSL dating of a coastal sediment sequence from the South Yellow Sea. Geochronometria 43, 143–154.
Gao, L., Long, H., Shen, J., Yu, G., Yin, Y., 2017. Optical dating of Holocene tidal deposits from the southwestern coast of the South Yellow Sea using different grain-size quartz fractions. J. Asian Earth Sci. 135, 155–165.
Guerin, G., Mercier, N., Nathan, R., Adamiec, C., Lefrais, Y., 2012. On the use of the infinite matrix assumption and associated concepts: a critical review. Radiat. Meas. 47, 778–785.
Hori, K., Saito, Y., 2007. An early Holocene sea-level jump and delta initiation. Geophys. Res. Lett. 34, L18401. http://dx.doi.org/10.1029/2007GL031029.
Hori, K., Saito, Y., Zhao, Q.H., Cheng, X.R., Wang, P.X., Sato, Y., Li, C.X., 2001. Sedimentary facies of the tide-dominated paleo-Changjiang (Yangtze) estuary during the last transgression. Mar. Geol. 177, 331–351.
Hori, K., Saito, Y., Zhao, Q.H., Wang, P., 2002. Evolution of the coastal depositional systems of the Changjiang (Yangtze) River in response to late Pleistocene-Holocene sea-level changes. J. Sediment. Res. 72, 884–897.
Huntley, D.J., Godfrey-Smith, D.I., Thewalt, M.L.M., 1985. Optical dating of sediments. Nature 313, 105–107.
Kim, J.C., Cheong, D., Shin, S., Park, Y.H., Hong, S.S., 2015. OSL chronology and accumulation rate of the Nakdong deltaic sediments, southeastern Korean Peninsula. Quat. Geochronol. 30, 245–250.
Kong, G.S., Lee, C.W., 2005. Marine reservoir corrections (ΔR) for southern coastal waters of Korea. Sea J. Kor. Soc. Oceanogr. 10, 124–128.
Lambeck, K., Rouby, H., Purcell, A., Sun, Y.Y., Sambridge, M., 2014. Sea level and global ice volumes from the last glacial maximum to the Holocene. Proc. Natl. Acad. Sci. U. S. A. 15296–15303.
Li, C.X., Chen, Q.Q., Zhang, J.Q., Yang, S.Y., Fan, D.D., 2000. Stratigraphy and paleoenvironmental changes in the Yangtze delta during Late Quaternary. J. Asia Earth Sci. 18, 453–469.
Li, X.X., Bianchi, T.S., Allison, M.A., Chapman, P., Mitra, S., Zhang, Z.R., Yang, G.P., Yu, Z.G., 2012. Composition, abundance and age of total organic carbon in surface sediments from the inner shelf of the East China Sea. Mar. Chem. 145–147, 37–52.
Liu, J.P., Xu, K.H., Li, A.C., Milliman, J.D., Velozzi, D.M., Xiao, S.B., Yang, Z.S., 2007. Flux and fate of Yangtze River sediment delivered to the East China Sea. Geomorphology 85, 208–224.
Madsen, A.T., Murray, A.S., Andersen, T.J., Pejrup, M., Breuning-Madsen, H., 2005. Optically stimulated luminescence dating of young estuarine sediments: a comparison with ^{210}Pb and ^{137}Cs dating. Mar. Geol. 214, 251–268.
Madsen, A.T., Murray, A.S., Andersen, T.J., Pejrup, M., 2007. Temporal changes of accretion rates on an estuarine salt marsh during the late Holocene — reflection of local sea level changes? The Wadden Sea, Denmark. Mar. Geol. 242, 221–233.
Marwick, T.R., Tamooh, F., Teodoru, C.R., Borges, A.V., Darchambeau, F., Bouillon, S., 2015. The age of river-transported carbon: a global perspective. Glob. Biogeochem. Cycles 29, 122–137.
Murray, A.S., Wintle, A.G., 2000. Luminescence dating of quartz using an improved single-aliquot regenerative-dose protocol. Radiat. Meas. 32, 57–73.
Murray, A.S., Wintle, A.G., 2003. The single aliquot regenerative dose protocol: potential for improvements in reliability. Radiat. Meas. 37, 377–381.
Olley, J.M., Caitcheon, G.G., Roberts, R.G., 1999. The origin of dose distributions in fluvial sediments, and the prospect of dating single grains from fluvial deposits using optically stimulated luminescence. Radiat. Meas. 30, 207–217.
Prescott, J.R., Hutton, J.T., 1994. Cosmic ray contributions to dose rates for luminescence and ESR dating: large depths and long-term time variations. Radiat. Meas. 23, 497–500.
Rees-Jones, J., 1995. Optical dating of young sediments using fine-grain quartz. Ancient TL 13, 9–14.
Reimer, P.J., Bard, E., Bayliss, A., Beck, J.W., Blackwell, P.G., Bronk Ramsey, C., Buck, C.E., Cheng, H., Edwards, R.L., Friedrich, M., Grootes, P.M., Guilderson, T.P., Haflidason, H., Hajdas, I., Hatté, C., Heaton, T.J., Hoffman, D.L., Hogg, A.G., Hughen, K.A., Kaiser, K.F., Kromer, B., Manning, S.W., Niu, M., Reimer, R.W., Richards, D.A., Scott, E.M., Southon, J.R., Staff, R.A., Turney, C.S.M., van der Plicht, J., 2013. IntCal13 and Marine13 radiocarbon age calibration curves 0–50,000 years cal BP. Radiocarbon 55, 1869–1887.
Shen, Z.X., Mauz, B., 2012. Optical dating of young deltaic deposits on a decadal time

scale. Quat. Geochronol. 10, 110–116.
Shen, Z.X., Törnqvist, T.E., Mauz, B., Chamberlain, E.L., Nijhuis, A.G., Sandoval, L., 2015. Episodic overbank deposition as a dominant mechanism of floodplain and delta-plain aggradation. Geology 43, 875–878.
Song, B., Li, Z., Saito, Y., Okuno, J., Li, Z., Lu, A.Q., Hua, D., Li, J., Li, Y.X., Nakashima, R., 2013. Initiation of the Changjiang (Yangtze) delta and its response to the mid-Holocene sea level change. Palaeogeogr. Palaeoclimatol. Palaeoecol. 388, 81–97 (Feng, Z.B., Liu, B.H., Zhao, Y.X.).
Southon, J., Kashgarian, M., Fontugne, M., Metivier, B., Yim, W.W.-S., 2002. Marine reservoir corrections for the Indian Ocean and Southeast Asia. Radiocarbon 44, 167–180.
Stanley, D.J., Chen, Z.Y., 2000. Radiocarbon dates in China's Holocene Yangtze Delta: record of sediment storage and reworking, not timing of deposition. J. Coast. Res. 16, 1126–1132.
Sugisaki, S., Buylaert, J.P., Murray, A.S., Tada, R., Zheng, H.B., Ke, W., Saito, K., Chao, L., Li, S.Y., Irino, T., 2015. OSL dating of fine-grained quartz from Holocene Yangtze delta sediments. Quat. Geochronol. 30, 226–232.
Tamura, T., Saito, Y., Nguyen, V.L., Ta, T.K.O., Bateman, M.D., Matsumoto, D., Yamashita, S., 2012. Origin and evolution of interdistributary delta plains; insights from Mekong River delta. Geology 40, 303–306.
Wallinga, J., 2002. Optically stimulated luminescenc e dating of fluvial deposits: a review. Boreas 31, 303–322.
Wang, X.C., Li, A.C., 2007. Preservation of black carbon in the shelf sediments of the East China Sea. Chin. Sci. Bull. 52, 3155–3161.
Wang, J., Guo, X., Xu, S., Li, P., Li, C., 1981. Evolution of the Holocene Changjiang delta. Acta Geol. Sin. 55, 67–81 (In Chinese with English abstract).
Wang, L.C., Chen, X.L., Chu, T.Q., 1997. A contrast analysis on the loads character of the Changjiang River and the Yellow River. Geogr. Res. 16 (In Chinese with English abstract), 71–79.
Wang, Z.H., Zhuang, C.C., Saito, Y., Chen, J., Zhan, Q., Wang, X.D., 2012. Early mid-Holocene sea-level change and coastal environmental response on the southern Yangtze delta plain, China: implications for the rise of Neolithic culture. Quat. Sci. Rev. 35, 51–62.
Wang, Z.H., Zhan, Q., Long, H.Y., Saito, Y., Gao, X.Q., Wu, X.X., Li, L., Zhao, Y.N., 2013. Early to mid-Holocene rapid sea-level rise and coastal response on the southern Yangtze delta plain, China. J. Quat. Sci. 28, 659–672.
Wang, Y., Long, H., Yi, L., Yang, L., Ye, X., Shen, J., 2015. OSL chronology of a sedimentary sequence from the inner-shelf of the East China Sea and its implication on post-glacial deposition history. Quat. Geochronol. 30, 282–287.
Yan, Q.S., Xu, S.X. (Eds.), 1987. Recent Yangtze Delta Deposit. East China Normal University Press, Shanghai (In Chinese with English abstract).
Yang, L., Long, H., Yi, L., Li, P., Wang, Y., Gao, L., Shen, J., 2015. Luminescence dating of marine sediments from the Japan Sea using quartz OSL and polymineral pIRIR signals of fine grains. Quat. Geochronol. 30, 257–263.
Yoneda, M., Uno, H., Shibata, Y., Suzuki, R., Kumamoto, Y., Yoshida, K., Sasaki, T., Suzuki, A., Kawahata, H., 2007. Radiocarbon marine reservoir ages in the western Pacific estimated by prebomb molluscan shells. Nucl. Inst. Methods Phys. Res. B 259, 432–437.